Resolving the structural complexity of γ-Al_2O_3: the nature of vacancy ordering and the structure of complex antiphase boundaries

Libor Kovarik[1*], Mark Bowden[1], Konstantin Khivantsev[1], Ja Hun Kwak[2], Janos Szanyi[1]

[1] *Institute for Integrated Catalysis, Pacific Northwest National Laboratory, P.O. Box 999, Richland, Washington 99352.*
[2] *School of Energy and Chemical Engineering, Ulsan National Institute of Science and Technology (UNIST), 50 UNIST-gil, Ulsan 44919, Republic of Korea.*

[*] *Corresponding author: libor.kovarik@pnnl.gov*

Abstract

The structure of γ-Al_2O_3 remains largely undetermined despite decades of research. This is due to the high degree of disorder, which poses significant challenges for structural analysis using conventional crystallographic approaches. Herein, we study the structure of γ-Al_2O_3 with Scanning Transmission Electron Microscopy (STEM) and ab-initio calculations to provide a complete structural description. We show that the microstructure can be understood in terms of two key structural features of nanoscale spinel domains and finite thickness segments termed as complex antiphase boundaries (cAPB) that provide the domain interconnectivity. The spinel domains have a distinctive preference for vacancy ordering, which can be rationalized in terms of a structure with a stacking disorder. Tetragonal $P4_12_12$ or monoclinic $P2_1$ models, all based on the identical motif, can be considered as representative ordered forms. Individual spinel domains are interconnected via cAPBs, which adopt a distinct non-spinel bonding environment of δ-Al_2O_3. The most common cAPB consists of a single delta motif with thickness of just 0.6 nm on (001), with the resulting displacement a/4 [101]. Remarkably, the cAPBs are shown to energetically stabilize the spinel domains of γ-Al_2O_3 explaining their high abundance. We demonstrate how the tetragonal distortions naturally arise in this intricate microstructure and place the proposed model in the context of phase transformations to high temperature transition aluminas.

1. Introduction

γ-Al_2O_3 is an important oxide with a broad use in several technological applications [1]. High thermal stability, high surface area, and advantageous surface properties make it particularly attractive for catalytic applications, where it has been used both as catalyst and catalytic support [2-5]. Despite decades of industrial use and active research, the basic structural characteristics of γ-Al_2O_3 remain actively debated [6-9]. This is largely due to a high degree of structural disorder.

The structural disorder encompasses several different types of defects and distortions, as relevant not only at the level of unit cell, but also at a larger scale [10-12]. The unit cell of γ-Al_2O_3 has been historically interpreted as defective spinel structure [13], which entails the introduction of vacancies to Al^{3+} sites, as dictated by the stoichiometry. Vacancies can occupy tetrahedral or/and octahedral Al sites, which are denoted as 8a and 16d Wyckoff sites of spinel Fd-3m structure [14]. Multiple studies based on NMR, XRD and TEM

addressed the topic of vacancy site preference, and a variety of different vacancy occupancy schemes were proposed, including the random or the preferred distribution of vacancies on either tetrahedral or octahedral Al^{3+}sites [15-18]. A theoretical approach based on the use of DFT methods has shown that vacancies should preferentially occupy octahedral sites [19, 20]. Several structural models based on vacancy ordering in octahedral sites have been proposed [21, 22].

The defective spinel models, with vacancies on Al^{3+} sites as the only "defective feature", have significant problems fitting X-ray/Neutron diffraction observations. Improvements were obtained by introducing $Al^{3+}$to non-spinel sites. These are sites other than 8a and 16d Wyckoff sites, or analogous sites in tetragonally distorted spinel [23]. For example, Zhou and Snyder [10] introduced a model with Al^{3+} occupying 25% of the 32e sites. More recent models by Paglia et al. [11] and Smrcok et. al. [24] assumed different non-spinel sites (16c,48f) in smaller proportions. The model proposed by Paglia et al. [11] also considered tetragonal lattice distortions. The structure was mapped onto $I4_1/amd$, which is the tetragonal maximal subgroup of Fd-3m. The modified spinel models, denoted here as "spinel-like" models, provide an improvement in fitting XRD/Neutron diffraction data, but any of such physical models would inevitably lead to the formation of sites with unacceptable nearest Al-Al distances. Thus, a physical basis for these models is lacking. In addition to spinel-like models, a fully non-spinel model has been proposed by Digne et al. [25]. The monoclinic ($P2_1/c$) structural model, which has now gained a wide acceptance in the catalysis community, has several characteristics that are difficult to justify in the light of recent experimental evidence [26].

While many previous studies focused on the rationalization of γ-Al_2O_3 structure/disorder within the context of the unit cell, it has been also well-realized that the defects and distortions extend beyond the unit cell. The key defects in this respect have been identified as faults that create nanoscale domains in the Al sublattice, while the oxygen sublattice remains coherent over larger scale. The first quantitative assessment of faulting in γ-Al_2O_3 derived from Boehmite was reported by Zhou and Snyder [10]. The extent of faulting was evaluated based on the non-uniform broadening of diffraction peaks. It is important to note that this work was preceded by TEM analysis, which identified a high density of faulting in plasma sprayed γ-Al_2O_3 samples [27]. Specifically, the faults were identified as antiphase boundaries (APBs) with the displacement a/4[110] on (100). Such results were later corroborated by TEM analysis of nanorod samples of γ-Al_2O_3 prepared by arc-discharge methods [28].

The disorder in γ-Al_2O_3 due to domains/APBs has been studied in recent years with the use of XRD Debye scattering approach as well as PDF analysis. The initial XRD Debye scattering work was performed by Tsybulya and Kryukova [29], and this was followed by more extensive work by Pakharukova et al. [8, 12] and by Rudolph et al. [9]. The use of Debye scattering approach has shown that the spinel domains should be very small, approaching the size of the spinel unit cell, such as 0.96x1.68x2.25nm [11], or 1.2x1.2x1.2nm [9]. The displacement vector for the APB was identified as ¼ [110]. The alternative displacement vector of ½ [100], which would also lead to APBs on Al sublattice, cannot reproduce the experimental XRD results [9]. PDF analysis has also argued in the favor of nanoscale domains [30]. It is noted that the PDF work by Paglia et al. [31] suggested the formation of faults in oxygen sublattice.

The Debye scattering modeling now strongly supports the concept of domains/APBs as the key structural feature of γ-Al_2O_3 [8, 9, 12]. However, the overall structure in these studies has been treated at a conceptual level with the key parameters unconstrained. This includes most importantly the vacancy ordering and the structure of APBs. To address the unresolved structural parameters of γ-Al_2O_3, we use HAADF atomic level imaging and DFT calculations. We demonstrate that γ-Al_2O_3 can be indeed interpreted as a domain microstructure of "defective spinel". We identify a strong preference for vacancy ordering in the spinel and show that the structure can be understood as a spinel analog of δ-Al_2O_3. The spinel domains themselves are interconnected by finite thickness APBs that adopt a δ-Al_2O_3 bonding environment. Remarkably, we show that such APBs can stabilize the overall spinel structure, rather than incur energetic penalty. The newly proposed structural model accounts for the tetragonal lattice distortions and provides a rationalization for the structural transformation of γ-Al_2O_3 into the more thermodynamically stable δ-Al_2O_3 and θ-Al_2O_3.

2. Experimental

The particles of γ-Al_2O_3 were synthesized from Boehmite prepared by alkoxide precipitation. Detailed description of Boehmite synthesis can be found in our previous work [32]. Transformation of Boehmite to γ-Al_2O_3 was performed in a tube furnace at 800°C for 2 hours.

Structural analysis was performed with aberration corrected Thermo-Fisher Themis Z Scanning/Transmission Electron Microscope (S/TEM). The observations were performed in Scanning mode using a HAADF detector. The probe convergence angle was 25 mrad, and the inner detection angle on the HAADF detector of 52 mrad. All images were collected using multi-frame integration, mostly consisting of 20 images. The acquisition and image processing were performed with Thermo-Fisher's Velox software.

The experimental observations were supported by image simulations performed with a computer code developed by E.J. Kirkland [33]. The simulation parameters were fixed to be consistent with the experimental acquisition conditions. The simulated images were convoluted with a Gaussian of FWHM=0.1 nm to account for spatial incoherence.

The energy stability of the proposed structures was evaluated with Density Functional Theory (DFT) approach using with Vienna Ab-initio Simulation Package (VASP) [34, 35]. Projector augmented wave (PAW) potentials and the Generalized Gradient Approximation (GGA) of Perdew and Wang (PW91) was used for the exchange correlation potential. Monkhorst−Pack scheme was employed for k-point sampling of the Brillouin zone. Plane-wave cutoff energy was 550 eV. All structures were allowed to fully relax. Atomic sites were relaxed to their equilibrium positions using a conjugate-gradient algorithm with the symmetry constrains of considered space group.

3. Results

3.1 TEM observations of γ-Al_2O_3

An example of the γ-Al_2O_3 microstructure, as revealed with atomic level STEM HAADF imaging along a direction consistent with spinel [110] is shown in Figure.1(a).

The image shows that the atomic structure is complex; it changes in an intertwined fashion across the field of view of several nanometers, which indicates that the structure may not be interpreted in terms of a single crystal but instead as an intertwined domain microstructure. In our observations we identify three main types of lattice contrast that define the overall microstructure. The three main types of lattice contrast are designated as type I,II,III, as shown in Figure.1(b,c,d). We note that the lattice contrast in the acquired images is often gradually changing, and that the type I, II, III can be often considered as the endpoints of this gradual change. In addition, the high density of nanoscale internal pores is another notable feature of the microstructure. The pores appear as darker regions that often disrupt lattice contrast.

In the type I lattice contrast (Figure.1(b), the atomic spacing and the relative intensities are consistent with that of spinel $[110]_{SP}$. The type II lattice contrast, shown in Figure.1(c), has a underlying connection to the spinel, but the relative intensities and the symmetry are inconsistent with $[110]_{SP}$ of the spinel. The contrast is dominated by one set of (111) lattice planes, with the spacing of 4.6A. There are two independent (111) types on $[110]_{SP}$, and these two orientations are observed with the same frequency. The type III contrast (Figure.1(d), has an underlying connection to the spinel structure but the atomic site intensities, and the resulting symmetry makes it inconsistent with that of a spinel in the $[110]_{SP}$ orientation.

The variability and complexity of HAADF Images represent a challenge for precise structural interpretation. For example, the overall variation in the lattice contrast can be interpreted in terms of both spinel and non-spinel ordering/domains being present. Alternatively, the structural complexity can be solely interpreted in terms of spinel domains, assuming the non-spinel contrast arises from the overlap of translationally related spinel domains. In the following text, we argue that the majority of non-spinel contrast, such as shown in Figure 1(c,d), indeed arises from the overlap of translationally related spinel domains. At the same time, we show that the microstructure also contains true non-spinel components. These non-spinel components are the finite thickness APBs that adopt a delta alumina bonding environment.

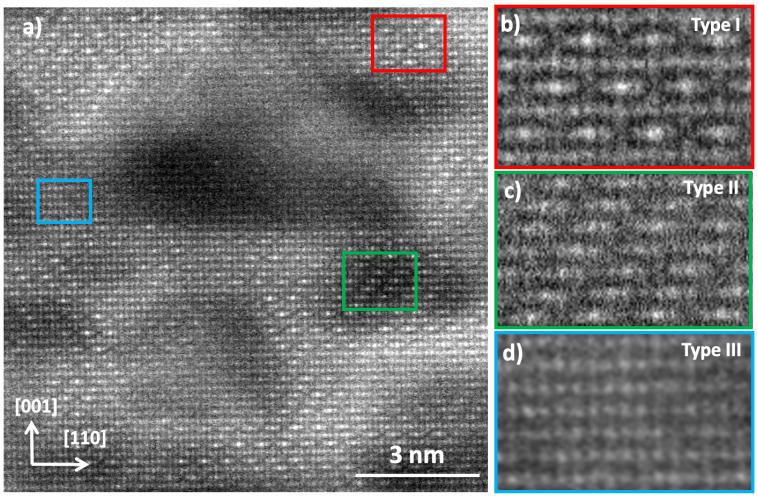

Figure 1. HAADF STEM observations of γ-Al_2O_3 along $[110]_{SP}$ orientation. (a) atomic view of the microstructure reveals the presence of domains. (b,c,d) Detail atomic level view

of the three types of image contrast, as prevalent on $[110]_{SP}$. (The magnified images in panels b,c,d are representative of the ordering contrasts but not extracted from panel a)

The non-spinel contrast of type II and III is interpreted in terms of through-thickness overlapping and translated spinel domains. The domain overlap is expected considering that the domain size is only few nanometers, which is smaller than the thickness of the studied samples, or the effective depth of focus in our STEM HAADF observations. The interpretation is also supported by the fact that the non-spinel contrast is often clearly observed in the regions between two phase-shifted type I domains, as shown in Figure 2(a), and that the formed contrast is consistent with the phase shift. In addition, the images often show a gradual change from type I to type II/III contrast, which would be expected for overlapping domains with boundaries inclined with respect to the observation direction.

A series of HAADF image simulations were performed to show that type II and III contrasts can indeed be formed by overlapping, mutually translated spinel domains. In particular, the type II lattice contrast is formed by two overlapping domains displaced by ¼[110], as shown in Figure 2(c). This type II contrast can be obtained with both conservative and non-conservative APBs and irrespective of the selection of the interfacial APB plane. Using two overlapping spinel domains, as the basis for the interpretation of HAADF images in Figure 1(c,d) and Figure2(a), appears as a good assumption given the current microstructure and the employed imaging conditions of probe convergence of 25mrad at 300kV. Given these conditions, the undisturbed depth of focus is ~5.5. nm, which would roughly correspond to two domains strongly controlling the atomic contrast in the HAADF images. To corroborate this, we performed HAADF simulations of thicker crystals. An example of HAADF image simulations from 9 nm crystal that consists of 3 domains, each of which under different shifts, is presented in Figure 2(d). Instead of obtaining an average contrast, the simulated image contrast is dictated by the two domains within the depth of focus. (Upper part of the crystal). The bottom domain is phase shifted in the opposite direction and would enhance the other set of (111) planes. The limited and tunable depth of focus in HAADF imaging is an important feature in studying the domain microstructure because it minimizes averaging through multiple domains (current γ-Al_2O_3 particle thickness is estimated to vary between ~20-30 nm omitting the internal porosity). This would be for example unavoidable in HRTEM imaging, which is additionally associated with the contrast reversal for thicker samples [36].

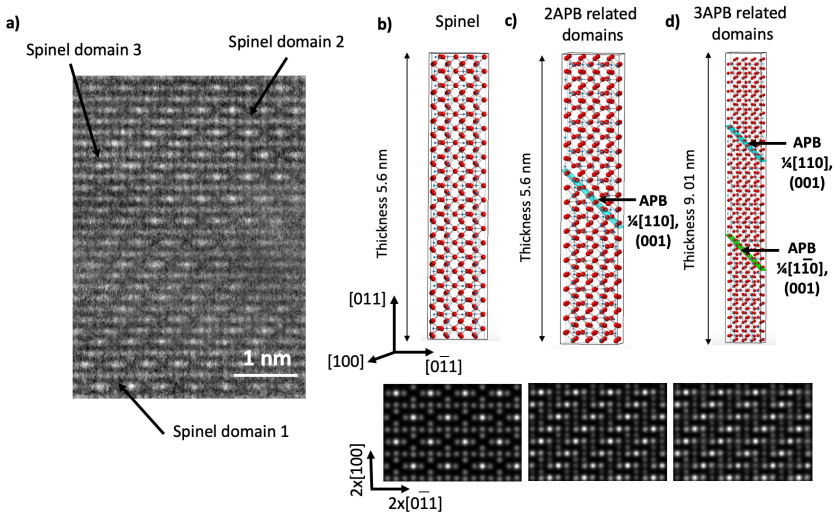

Figure 2 (a) HAADF observation of γ-Al_2O_3 along $[110]_{SP}$ revealing the presence of several spinel domains. (b) Structural model and corresponding HAADF simulation of reference spinel structure. (c) Structural model and corresponding HAADF simulation of two overlapping APB related domains. (d) Structural model and corresponding HAADF simulation of three overlapping APB domains, each of which with different shift.

For type III contrast, a full reproduction can be obtained from the overlapping domains that are phase shifted either by 1/4[110], or by 1/2[100]. In the case of phase shift ¼[110], the APB would have to be non-conservative. For example APB (001) with b=¼[101] observed along [10-1] can reproduce the type III contrast. Interestingly, it is noted that a non-conservative APB with b=¼[101] as viewed along the displacement direction leaves the spinel domains in projected registry, and thus type I contrast. Accounting for this may be an important tool for proper interpretation of domain size in STEM images.

True non-spinel components are also present in the microstructure, and they are revealed as finite thickness antiphase boundaries. An example of well-resolved finite thickness APB on {001} in an edge-on orientation is shown in Figure 3(a). Structurally, the APB can be interpreted as single δ-Al_2O_3 motif with thickness of 0.6 nm interfaced between two spinel domains on (001) plane. The δ-Al_2O_3 motif has been previously defined in our earlier work and shown to be the basic building block of intergrowth in $\delta_{2,3,4}$-Al_2O_3 [37, 38]. The atomic model depicting the single delta motif incorporated between two spinel domains is shown in Figure 3(c). The delta motif incorporated into the spinel on (001) has full compatibility in terms of octahedral and tetrahedral sites. It will be shown that in the context of proposed spinel vacancy ordering scheme, it can accomplish a full intergrowth, and this is the basis of highly stable configuration. The corresponding HAADF simulation is shown in Figure 3(b).

The finite thickness APB on (001) leads to displacement between the spinel domains that is defined as b=1/4 [101] using the reference frame of spinel. The displacement vector has out of plane component, which would be consistent with a non-conservative APB. However, the APB has finite thickness, unique structure and does not lead to local stoichiometry modifications. This makes it distinguishable from the non-conservative APB. Because of these considerations, in this work we use the terminology “complex APBs”

(cAPB) to distinguishes it from the conventional conservative or non-conservative APBs [39].

The cAPB are key component of the microstructure. In addition, we also observed thicker cAPBs corresponding to two delta motifs on (001), although at lower frequency. For cAPBs with thickness of two delta motifs, the displacement vector should correspond to b=1/2[001]. This is because the stacking of two delta motifs involves rotation and shifts [38], and the vector simply does not correspond to doubling of single delta motif of b=1/4[101].

The cAPBs can be also identified along other planes/boundaries, most of which do not align with the rational low-index planes. An example of the complex APB with the boundary inclined with respect to the (110) plane is shown in Figure 3(d). The characteristic δ-Al_2O_3 segments can be clearly identified as the boundary between two offset spinel domains. At the present time, the obtained images from these cAPB don't provide the necessary details to construct the full atomic model.

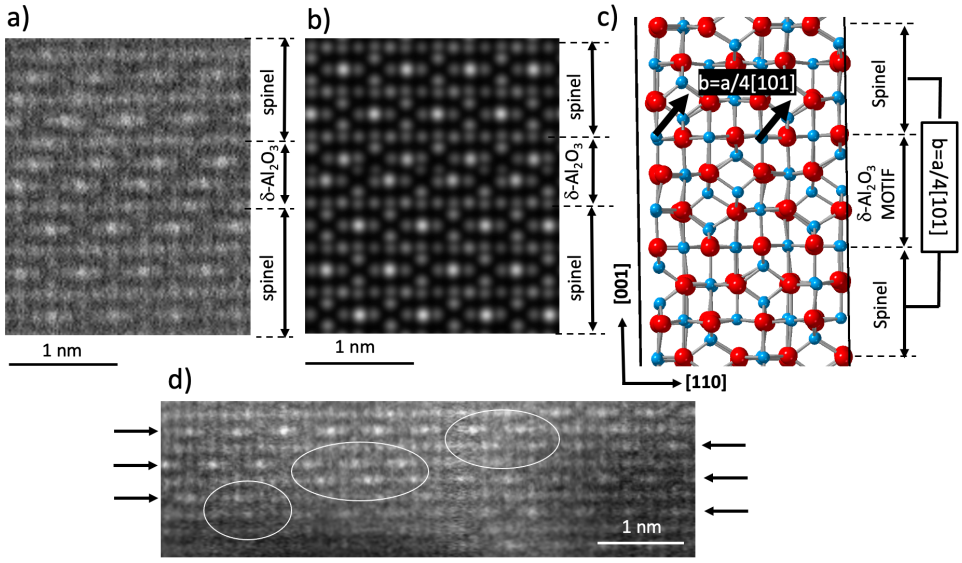

Figure.3. (a) HAADF STEM observation of cAPB (delta motif) in γ-Al_2O_3 on (001) as viewed in the edge on orientation. (b) HAADF simulation of spinel structure containing delta motif leading to cAPB (c) Atomic model of cAPB created by delta motif gives rise to ¼[(001) in the spinel structure. (d) HAADF STEM images of γ-Al_2O_3 with cAPB on irrational plane.

The current microstructure can be generally interpreted as a domain microstructure. Overall, the morphology and the size of the spinel domains is difficult to quantify given the convoluted character of obtained images. Nevertheless, it can be concluded that the size of spinel domains is often smaller in the perpendicular direction to cAPBs. The lower limit of thickness is 0.6 nm, which corresponds to single spinel motif intergrown with delta motifs. An example of such structure is shown in Figure. 4(a). Note that in these instances, the structure can be better understood as mutual intergrowth of spinel and delta motifs rather than a domain structure. On the other hand, there are domains which are more equiaxed and that reach over 3 nm in size. In addition, we have also identified some

instances of 1-2 nm δ-Al_2O_3 domains. This indicates that δ-Al_2O_3 starts to form well before the appearance of characteristics XRD peaks, and it can represent as part of what is generally understood as the γ-Al_2O_3 structure.

The microstructure was also investigated along other crystallographic directions. The other examined directions, such as $[100]_{SP}$, don't reveal any domain information. In Figure 4(b), we show an observation from $[100]_{SP}$ that display uniform lattice contrast without domains or superlattice contrast of spinel. This is interpreted as due to multiple phase-shifted domains being within the depth of focus, and effectively averaging the contrast in the projection. In addition, we point out that the structure lacks faults/defects in the oxygen sublattice across the distance of several tens of nm.

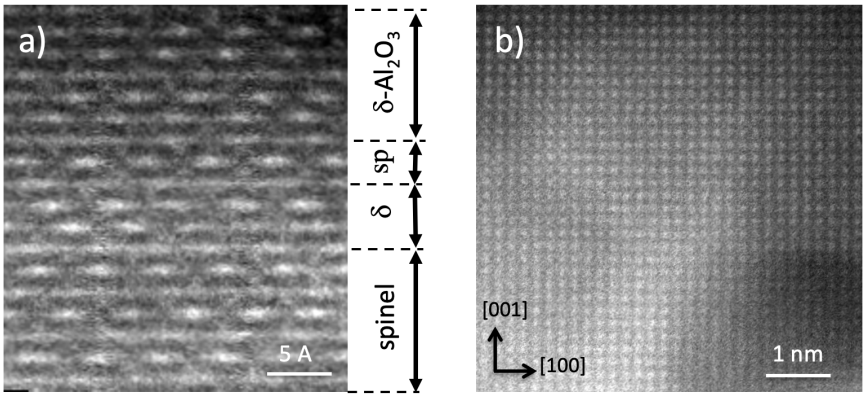

Figure 4. (a) HAADF STEM observations of γ-Al_2O_3 from [110] revealing an intergrowth of spinel and delta motifs, each of which can be only is 0.6 nm in thickness. (b) HAADF STEM images of γ-Al_2O_3 as obtained from [100].

3.2. Vacancy ordering within the spinel domains of γ-Al_2O_3

The vacancy ordering/distribution in the spinel domains represents a key structural parameter of γ-Al_2O_3. The topic of vacancy ordering is difficult to address purely on the basis of the experimental observations. This is because the experimental observations, including HAADF imaging, do not directly point to any specific ordering scheme. Few exceptions from HAADF imaging exist, where the images show weak evidence of vacancy ordering. This is identified with the arrows in the largest domains of Figure 5.

The general lack of ordering contrast can be interpreted either in terms of random distribution of vacancies, or alternatively in terms of vacancy short-range ordering (VSRO), which means that the vacancy ordering is realized locally in small pockets (subdomains). Depending on the extent of VSRO, the ordering contrast may be significantly attenuated and thus not accessible in STEM. It is pointed out that the general complexity of the microstructure alone can be argued to play an important role attenuating the vacancy ordering contrast.

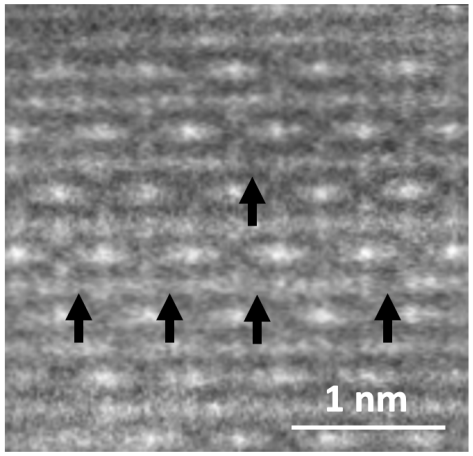

Figure 5. HAADF observations of large γ-Al_2O_3 domain. A subtle contrast variation can be identified in a subset of octahedral sites, indicating a preference for vacancy ordering.

A strong argument for ordering/VSRO being present can be put forward based on the energetic stability. In the context of γ-Al_2O_3, the energetic stability is controlled by two main terms. One is naturally the stability of the bulk spinel structure/vacancy ordering. The second term relates to the energy stability of cAPBs in the spinel, which is an important factor for γ-Al_2O_3 because of their high density. Both terms combined control the overall structural stability.

We show that there exists a vacancy ordering scheme that not only has the highest bulk energetic stability, but at the same time also has the highest compatibility/stability with cAPBs, which remarkably leads to the stabilization of the structure. In other words, cAPB leads to a negative cAPB energy. As both terms support this vacancy ordering model independently, with resulting high stability, a strong case can be made in comparison with other possible types of ordering, or random distribution of vacancies.

The identified spinel ordering can be best described as a spinel analog of δ-Al_2O_3 [37, 38]. The key analogous feature is that the structure can be rationalized in terms of structure with a stacking degree of freedom [38, 40]. (It is noted that the stacking degree of freedom does not represent the VSRO subdomains, which arises yet from another ordering violation). The structure can be described in terms of the basic stacking motif and stacking rules. The basic stacking motif of γ-Al_2O_3 is shown in Figure.6(a). It is identical in size with δ-Al_2O_3 as shown in Figure.6(b). The additional analogous features with δ-Al_2O_3 includes occupation of Al^{3+}, which can be for example well seen from the occupation of octahedral Al^{3+}. Every third (001) is fully occupied (4 atoms). The remaining two (001) planes are occupied with 3 octahedral Al^{3+}. The resulting occupation sequence in the basic motif (γ-Al_2O_3 or δ-Al_2O_3) can be then represented as 433. Moreover, the Al^{3+}/vacancy distribution is fully identical across two (001), as highlighted in Figure 6(a,b). The third (001) plane breaks the pattern of similarity. In spinel motif, the Al^{3+} atoms (octahedral/tetrahedral) are restricted to spinel sites, and this is not the case in the δ-Al_2O_3 motif. We note that in the stacked configuration, the fully identical sequence extends beyond (prior) the basic motif and can be expressed as 343.

Several crystallographic variants can be formed by vertical stacking of the spinel basic motif in a periodic fashion. The two most energetically stable crystallographic variants are

the tetragonal $P4_12_12$ (No.92) and the monoclinic $P2_1$ (No.9). In the case of the $P4_12_12$ structure (Figure 6(c)), the stacking is formed by 90-degree related motifs. In the case of the monoclinic $P2_1$ structure it is formed by stacking of 180-degree rotation and inversion of related motifs. This latter structure (Figure 5(d)) has 2-fold screw axis along the non-stacking direction. Other models using different stacking operations have been also identified as energetically favorable. It is noted that the spinel ordering of $P4_12_12$ structure has been determined as the most stable ordering schemes for γ-Fe_2O_3 [41, 42], which has been historically considered as closely related to γ-Al_2O_3 [6, 13].

The spinel motif can fully intergrow with δ-Al_2O_3 on (001), which is the basis of the cAPB with high stability (negative cAPB energy). The intergrowth occurs when γ-Al_2O_3 and δ-Al_2O_3 motifs are in a distinct translational (intergrowth) relationship. Accommodating such a relationship among multiple domains in 3D may not be possible without introducing some break in the order. The VSRO subdomains may thus be expected to arise from compatibility requirements imposed by cAPBs. We note that when the thickness of spinel domains is very small, as observed in Figure 4(a), the domains are expected to be mostly free of VSRO. Interestingly, we point out that the thickness of domains is often smaller than the c lattice parameter of the tetragonal $P4_12_12$, and in some case even the monoclinic $P2_1$ structure.

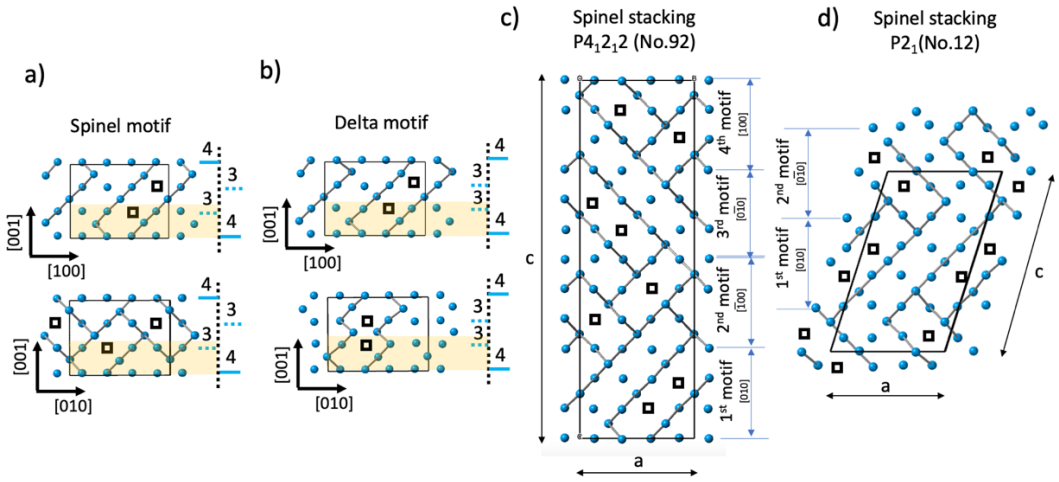

Figure.6. (a) Vacancy ordering in γ-Al_2O_3 domains can be explained as intergrowth structure based on a spinel motif. Basic motif of γ-Al_2O_3 as viewed along the [010] and [100]. (b) The basic motif of δ-Al_2O_3 (the basis of cAPB in γ-Al_2O_3 structure). Both delta and spinel motif can be considered as closely analogous. (c) Spinel based structure $P4_12_12$ (No.92) based on four spinel motifs (d) Spinel structure S.G. $P2_1$ (No.12) based on two basic spinel motifs. In all models, only Al^{3+} are visualized. Vacancies are visualized as squares.

3.2.1. Energetic stability of vacancy ordering in γ-Al_2O_3

The calculated formation energy of vacancy ordered structure with $P4_12_12$ symmetry (or its enantiomorphic counterpart $P4_32_12$) (ΔE_γ-ΔE_{alpha}) is 0.084 eV/Al_2O_3. The stacking

sequence of $P2_1$ structure has a slightly higher formation energy (ΔE_γ-ΔE_{alpha}) of 0.091 eV/Al_2O_3, which can be essentially considered as energetically degenerate.

Spinel models with random distribution of vacancies on Al^{3+} octahedral sites have a significantly higher formation energy. In the case of average Fd-3m structures, where vacancies are allowed for all octahedral sites, but without allowing to be nearest neighbors, the formation energy was calculated as (ΔE_γ-ΔE_{alpha}) = 0.201 eV/Al_2O_3. This value was estimated from 10 randomly seeded configurations with the total of 640 atoms. The variation among the models is 0.167-0.272 eV/Al_2O_3. We also evaluated the formation energy in the context of cubic $P4_332$ (No.212) structure, which accommodates three different Al^{3+}sites. For vacancies constrained only to 4b site, which results in a structure that is closely related to the tetragonal model $P4_12_12$ (or $P4_32_12$) [41, 43], the average formation energy was evaluated as (ΔH_γ-ΔH_{alpha}) = 0.175 eV/Al_2O_3. The variation for (ΔE_γ-ΔE_{alpha}) is 0.154-0.202 eV/Al_2O_3 among the 10 randomly seeded configurations of 640 atoms. Significantly higher formation energy for the random distribution provides strong argument for vacancy ordering. It is important to point out that the vacancy short-range order will naturally tend to lower the energetic preference. At the same time, the formed sub-domains of VSRO are expected to facilitate structural compatibility of cAPBs and thus minimize the interfacial energy.

The previously proposed spinel models of γ-Al_2O_3 have higher formation energy. The model proposed by Menendez et al. [22] has the energy of formation of (ΔE_γ-ΔE_{alpha})=0.21 eV/Al_2O_3. The non-spinel model by Digne at al.[25] has the energy of formation (ΔE_γ-ΔE_{alpha}) = 0.14 eV/Al_2O_3.

In comparison, the structures of δ-Al_2O_3 and θ-Al_2O_3 are significantly more stable. For δ-Al_2O_3, the average energy of formation is (ΔE_δ-ΔE_{alpha})=0.052 eV/Al_2O_3 [38, 40]. The defect free structure of θ-Al_2O_3 has the energy of formation (ΔE_θ-ΔE_{alpha}) = 0.050 eV/Al_2O_3 [44]. The comparison of stability for the identified ordering variants of γ-Al_2O_3, together with the stability of other relevant structures/polymorphs of Al_2O_3, is plotted in Figure 7.

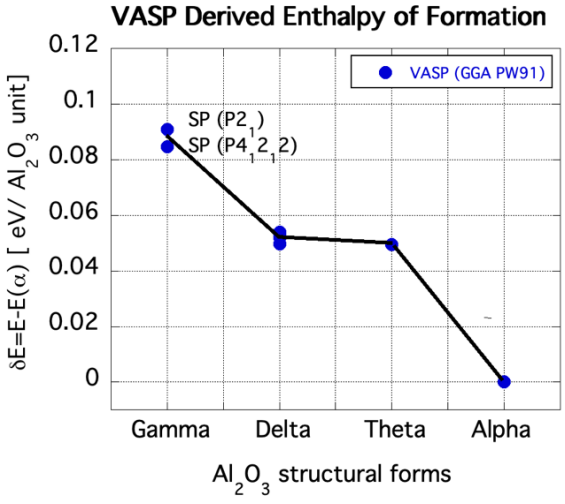

Figure 7. DFT derived energy of formation for the two newly proposed structural forms of γ-Al_2O_3, and other structural forms, including δ-Al_2O_3, θ-Al_2O_3 and α-Al_2O_3.

3.2.2. Energetic stability of cAPB in γ-Al_2O_3

The cAPBs are created by introduction of delta motifs in the spinel on the (001) planes. One of the key findings of this study is that the delta motif can form in a highly compatible fashion (intergrowth) in the spinel, which indicates that cAPBs are highly stable. Here we evaluate and discuss the energetic stability of cAPBs based on DFT calculations.

The most stable configuration for cAPB is obtained for full structural intergrowth, which is defined as $(001)_{SP1}//(001)_{\delta}//(001)_{SP2,}$ with additional translational/termination requirement. An example of two cAPB configurations with different ratios of spinel to delta motifs is shown in Figure 8(a,b). DFT calculations show that under such conditions, the cAPB does not introduce an energetic penalty, but instead stabilizes the spinel structure. The calculated cAPB energies are -47 mJ/m^2 and -44 mJ/m^2 for the two super-cell configurations in Figure 8(a,b). The results can fully rationalize the high density of cAPBs in γ-Al_2O_3. It is interesting to point out that the introduction of cAPB leads to the formation of an enantiomorphic couple of $P4_12_12$ (No.92) and $P4_32_12$ (No.96), as evident from the configuration in Figure 8(b).

The general configurational space for creation of cAPB in spinel on (001) goes beyond the previously specified intergrowth. This includes configurations such as $[001]_{SP1}//[001]_{SP2}$ on (100) planes, or between rotationally related motifs, such as $[001]_{SP1}/[010]_{SP2}$ and $(001)_{SP1}/(010)_{SP2}$ or $[001]_{SP1}/[010]_{SP2}$ and $(010)_{SP1}/(010)_{SP2}$. In each case, an additional degree of freedom exists because of large degree of freedom for translation/termination. Consequently, there is great number of possible configurations, but in each case the vacancy sites in γ-Al_2O_3 and δ-Al_2O_3 motifs cannot be perfectly shared. Nevertheless, some of the cAPB configurations can have a relatively low energy. An example of low energy configuration, defined by $(100)_{SP1}$/cAPB/$(100)_{S2}$ is shown in Figure 8(c). The calculated cAPB energy is 68 mJ/m^2. Another set of expected low energy cAPB configurations involve 90-degree related motifs, such as $(100)_{SP1}$/cAPB/$(001)_{SP2}$. A seamless intergrowth of γ-Al_2O_3 and δ-Al_2O_3 motifs can be achieved for one of the domains.

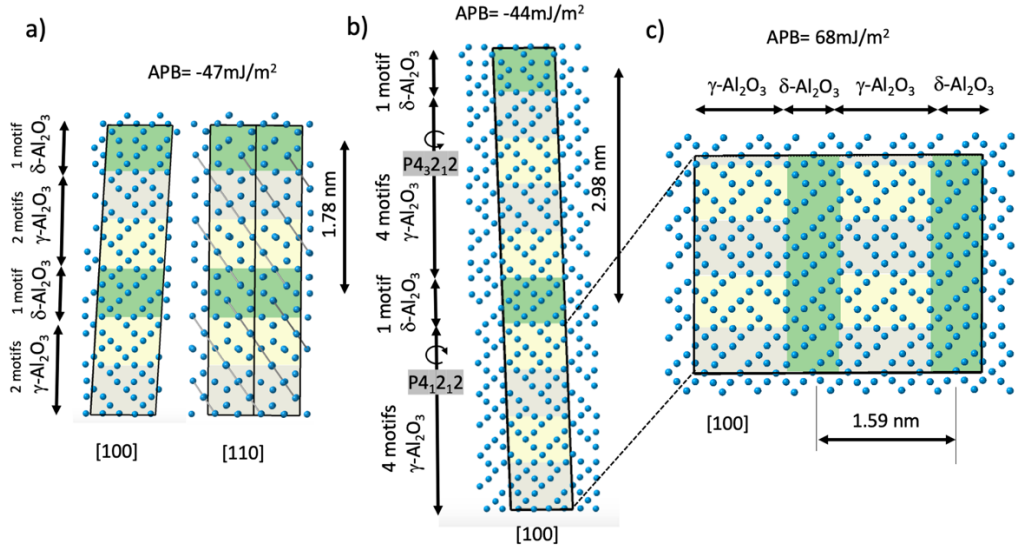

Figure 8. Supercell of γ-Al_2O_3 structure based on spinel domains (light color) separated by cAPBs (delta motif, green). (a) The supercell structure based on a ratio of two spinel motifs

to one delta motif (cAPBs) on (001) (b). The supercell structure based on a ratio of four spinel motifs to one delta motif (cAPBs) on (001). Introduction of cAPB leads to the formation of enantiomorphic couple of $P4_12_12$ (No.92) and $P4_32_12$ (No.96). (c) The supercell spinel structure with cAPBs on (010) interface.

3.3. Tetragonal distortions of γ-Al_2O_3

It is well known that the structures of γ-Al_2O_3 exhibit tetragonal lattice distortions that varies depending on the heat treatment and the nature of precursor used [45]. In some cases, the tetragonal distortions can be negligible with (c/a) ratio of ~1, or on the other hand it can be significant with c/a ratio of ~0.990, such as for example seen for 2 hours@800˚C sample in Figure 9(a). The currently proposed model of γ-Al_2O_3 has the necessary attributes to explain the tetragonal lattice distortions. In comparison, conventional defective spinel structures have a relatively negligible tetragonal lattice distortions, and do not have the ability to explain the experimental observations.

We find that the tetragonal lattice distortions in the structural model of γ-Al_2O_3 are derived mostly from the strain imparted by the complex APBs (δ-Al_2O_3 motif). Assessment of the tetragonal distortions was performed with the use of DFT calculations for the model configurations presented in Figure 8. Naturally, we find that the higher the density of cAPBs the higher degree of tetragonal distortions. For a configuration with the domain thickness of 1.78 nm, the estimated tetragonal distortion is c/a=0.992. For the larger spinel domain of 2.98 nm, as shown in Figure 8(b), the tetragonal lattice distortions are less pronounced of c/a =0.994. For comparison, the tetragonal distortions of $P4_12_12$ is small with c/a ratio of 0.998.

The present calculations only account for horizontal cAPBs. Higher degree of distortions can be expected if we account for vertical cAPB aligned in the same direction, or if cAPBs are thicker. On the other hand, when cAPBs are aligned perpendicular to the stacking directions, as shown in Figure 8(c), the overall lattice distortions would cancel out. In general, the degree of tetragonal distortions in the present model are controlled by the domain size, shape and orientation of cAPB.

It is interesting to point out that for the configuration in Figure 8(c), the tetragonal distortion is controlled by the cAPBs despite the opposite native tetragonal distortion of defective spinel. For domain spacings of 1.59nm, the distortion is c/a = 0.995. We note that the true distortions in this case are orthorhombic but are averaged for comparison purposes. The simulated XRD patterns from all the configurations discussed above are shown in Figure 9(b). The simulation includes the 2theta range around $(400)_{sp}$ peak, which well depicts the tetragonal distortions. The presented calculations assume peak broadening corresponding to particles size of 40 nm. The simulated $(400)_{sp}$ from the $P4_12_12$ defective spinel is also shown for comparison purposes: the tetragonal distortions are not discernable given the peak broadening parameter.

The tetragonal distortions further propagate in the microstructure heat treated to temperatures exceeding 800˚C, as γ-Al_2O_3 gradually transforms to δ-Al_2O_3 and θ-Al_2O_3 [46, 47]. In such conditions, it is expected that the fraction of cAPBs with higher thickness (two delta motifs) increases, which leads to more tetragonal distortions. It is also clear that when the small pockets of δ-Al_2O_3 evolve, this further increase the distortion. The gradual form of this transformation is fully consistent with the present structural model.

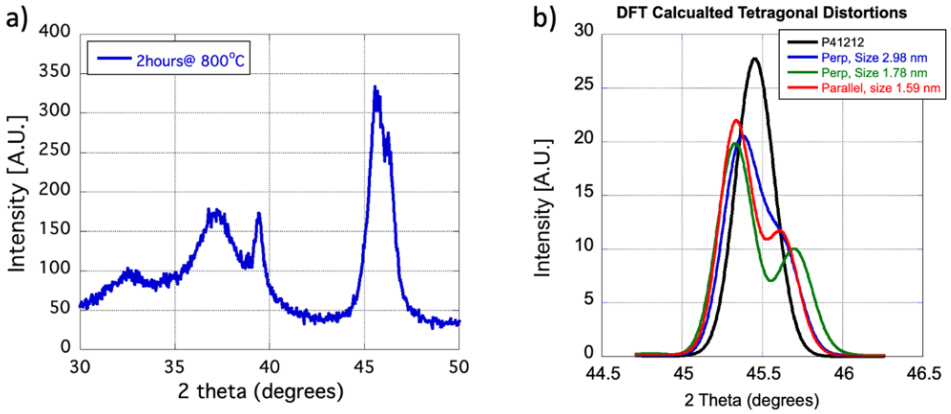

Figure. 9 (a) Experimentally measured XRD patterns of γ-Al_2O_3 heat treated at 800°C for 2 hours. (b) Simulated XRD patterns for (400) of γ-Al_2O_3 for structures obtained from DFT.

3.4. Octahedral/tetrahedral ratio in γ-Al_2O_3

The proportion of Al^{3+} octa- and tetrahedral sites represents an important structural parameter of γ-Al_2O_3. This parameter has been associated with some controversies in the past, as the experimentally determined values have been reported to have rather a broad range. The fraction of tetrahedral sites has been reported as low as ~21% [46], and as high as 36.5 % [48]. The broad range was discussed on several occasions [6, 49]. It has been pointed out that the lowest reported range of 21-30% may not reflect well the actual percentages [46, 50].These values were obtained from lower field NMR measurements and with magic angle spinning (MAS) of ~10MHz, where the conditions are not sufficient to adequately resolve all Aluminum sites [6, 49]. The work based on high field NMR measurement indicates higher percentage (~30-36.5%) of tetrahedral sites [36, 48, 51, 52], which can be considered as representative of γ-Al_2O_3.

The highest reported values of 36.5 % [48] is consistent with the present structural model, which considers vacancies exclusively populating octahedral sites. This translates to 37.5% of tetrahedral and 62.5% octahedral sites. The current model is, however, less consistent with the lower range of tetrahedral sites (~30%). We believe that a full consistency can be achieved if we account for other features/defects that are expected to modify the proportion of tetrahedral/octahedral sites. Surfaces are expected to be the most prominent features, contributing more profoundly for materials with higher surface area. This is because surfaces are known to undergo significant reconstructions, with expected change in proportion of octahedral/tetrahedral sites [32, 36]. Experimental evidence points to the surfaces as the factor affecting the octahedral/tetrahedral ratio. The work on lower surface area aluminas indicates 35.4-36.5 % of tetrahedral sites [36, 48], while the work on high surface area (SBA-200) indicates a lower percentage of 30-34.8 % tetrahedral sites [36, 51]. Defects associated with cAPBs can be envisaged as another factor modifying the proportion of tetrahedral/octahedral sites. This may include junction points of cAPBs, triple point boundaries, and also cAPBs defined by low-index or irrational planes. Octahedral Al^{3+} sites can be expected to be favored in such sites as they have higher degree of freedom for their accommodation.

4. Discussion

The current study addressed the complexity of γ-Al_2O_3 structure including the vacancy ordering in spinel domains, and the nature of cAPBs. These are the two defining parameters for γ-Al_2O_3 derived from thermal decomposition of Boehmite. For samples derived by other preparation methods, such as plasma spray or thermal oxidation, the cAPBs are present at lower densities [27, 53, 54], and the key structural parameter can ultimately become only vacancy ordering in the defective spinel.

The γ-Al_2O_3 systems, such as those prepared by deposition techniques [27, 53, 54] have a low density of faults and this could potentially prove invaluable for experimentally addressing the asserted vacancy ordering in the defective spinel structure. The present study argues in the form of well-defined ordering, but with the flexibility afforded by stacking degree of freedom and formation of VSRO subdomains, which breaks a long-range periodicity. This contrasts to random distribution of vacancies. The experimental effort to understand the vacancy ordering should be also complemented by theoretical approaches, with the focus on full stability calculations at relevant state conditions. To address this topic, it will be yet required to fully define the VSRO, which remained largely unexplored in this work. We note that our preliminary data show that VSRO subdomains can be well accommodated in a common microstructure in low energy configurations, which is an important prerequisite for their formation. In addition, the theoretical calculations should also account for the constrains from cAPB, as well other such as free surfaces.

The domain structure having a stacking degree of freedom and VSRO subdomains can be effectively represented in terms of partial occupancy models. The selection of crystal system for the representation can be expected to vary depending on the actual stacking variation and VSRO subdomains. In the most general form, the domain structure can be ultimately represented in terms of partial occupancy of Fd-3m system, where vacancies are limited to 16d octahedral sites. Such representation would be consistent with the interpretations previously considered for γ-Al_2O_3, although with vacancies not exclusively limited to octahedral sites. The proposed ordering variation cannot be represented in terms of spinel-like models, where Al^{3+} is partially present on non-spinel sites [10, 11, 24]. Non-spinel sites only arise at the cAPBs (delta segments) and neighboring domains.

The nature of ordering in spinel domains of γ-Al_2O_3 can be alternatively also addressed by studying its closely related systems, such as γ-Fe_2O_3. Both the spinel domains of γ-Al_2O_3 and the structure of γ-Fe_2O_3 appear to be driven towards the identical ordering type of $P4_12_12$ [41] (or its enantiomorphic counterpart $P4_32_12$ [43]), which suggests that the same disorder features may be also present. In the case of γ-Fe_2O_3, the disorder has been rationalized in terms of partial occupancy models. In addition to a fully ordered state of $P4_12_12$, which can be conveniently achieved for larger nanoparticles [55], the more disordered states have been shown to adopt either cubic $P4_332$ [42], or tetragonal $P4_32_12$ partial occupancy, or cubic spinel Fd-3m model with vacancies occupying octahedral 16d sites [56]. It will be worthwhile to examine whether the concept of stacking disorder/VSRO subdomains can be applied for physical representation of these various less-ordered states in γ-Fe_2O_3, and whether this in return can be used to understand the less accessible γ-Al_2O_3. It is noted that in the recent work on off-stochiometric γ-Fe_2O_{3-x}, the concept of local ordering has been proposed to interpret the attenuated superlattice intensities [42]. The

domains were envisioned to adopt partial occupancy $P4_332$ structure, which distinguish it from the present interpretation.

In addition to vacancy ordering, the variations in the structure of cAPBs under non-intergrowth arrangement will require further studies. The intergrowth type of cAPBs forms on cube (001) planes and leads to displacement vector of b=1/4 [101]. It is noted that this is consistent with the conceptually defined APB on (001) with b=1/4 [101] as previously identified by Dauger and Fargeot in TEM [27], and by Rudolph et. al [9] from XRD. The cAPBs with larger thickness of two delta motifs should have displacement vector corresponding to b=1/2[100], assuming conventional stacking between the two delta motifs. We note that it is also possible to create the alternative stacking configuration, which would lead to a displacement b=1/2[110] between the domains. The modified stacking of delta motifs is not hypothetical, but has been previously observed in the form of nanoscale segments in θ-Al_2O_3 [57]. The cAPBs with b=1/2[110] would result in "spinel-registry" between the adjacent domains. Consequently, their presence would be detectable only in "edge-on" orientation. Our DFT calculations show that such alternative stacking of delta motifs for cAPB is energetically degenerate with the identified spinel ordering. Any cAPB with thickness of three or more delta motifs can be more appropriately interpreted as δ-Al_2O_3. It is expected that such configurations become more prevalent as γ-Al_2O_3 gradually transforms to high temperature polymorphs. The cAPBs defined by irrational planes have been identified in the current work as important part of the microstructure and should be the subject of further studies.

5. Conclusions

The structure of γ-Al_2O_3 was investigated using HAADF imaging and DFT calculations. We show that γ-Al_2O_3 can be described as a complex structure consisting of the spinel domains interconnected with high density complex APBs. We propose a vacancy ordering in the spinel domains, which can be considered as the spinel analog of δ-Al_2O_3. The analogy arises from the stacking degree of freedom and the high degree of similarity between the basic stacking motifs. A periodic stacking of the basic spinel motifs would lead to tetragonal $P4_12_12$ or monoclinic $P2_1$ models. The finite thickness complex APBs are the key feature of the γ-Al_2O_3 microstructure. The bonding environment of these cAPB is found to be consistent with that of δ-Al_2O_3. The most common type has thickness of 0.6 nm and leads to displacement a/4 [101] on (001). We found that such APBs can stabilize the spinel microstructure rather than introduce an energetic penalty. The proposed model can fully rationalize the tetragonal distortions experimentally observed for the γ-Al_2O_3 microstructure. In addition, we reveal that the model has the necessary characteristics to explain the gradual transformation of γ-Al_2O_3 into high temperature transition aluminas.

Acknowledgements: The work was supported by the U.S. Department of Energy, Office of Science, Basic Energy Sciences, Chemical Sciences, Geosciences, and Biosciences Division, Catalysis Science program, FWP 47319. PNNL is a multi-program national laboratory operated for DOE by Battelle.

References:

[1] L.K. Hudson, C. Misra, A.J. Perrotta, K. Wefers, F.S. Williams, Aluminum Oxide, Wiley-VCH Verlag GmbH & Co. KGaA, Weinheim, Germany, 2000.
[2] G. Busca, Structural, Surface, and Catalytic Properties of Aluminas, Advances in Catalysis, 57 (2014) 319-404.
[3] M. Trueba, S. Trasatti, γ-Alumina as a Support for Catalysts: A Review of Fundamental Aspects, Eur. J. Inorg. Chem., 2005 (2005) 3393-3403.
[4] R. Prins, A. Wang, X. Li, Introduction to Heterogeneous Catalysis, World Scientific Publishing Company, 2016.
[5] J.H. Kwak, J. Hu, D. Mei, C.-W. Yi, D.H. Kim, C.H.F. Peden, L.F. Allard, J. Szanyi, Coordinatively Unsaturated Al3+ Centers as Binding Sites for Active Catalyst Phases of Platinum on γ-Al2O3, Science, 325 (2009) 1670-1673.
[6] R. Prins, On the structure of γ-Al2O3, Journal of Catalysis, 392 (2020) 336-346.
[7] A.L. Clauser, K.O. Sarfo, R. Giulian, C. Ophus, J. Ciston, L. Árnadóttir, M.K. Santala, Characterization of the atomic-level structure of γ-alumina and (111) Pt/γ-alumina interfaces, Acta Materialia, 245 (2023) 118609.
[8] V.P. Pakharukova, D.A. Yatsenko, E.Y. Gerasimov, S.V. Tsybulya, A study of γ-Al2O3 from the viewpoint of 3D nanostructure, Journal of Solid State Chemistry, 302 (2021) 122425.
[9] M. Rudolph, M. Motylenko, D. Rafaja, Structure model of γ-Al2O3 based on planar defects, IUCrJ, 6 (2019) 116-127.
[10] R.-S. Zhou, R.L. Snyder, Structures and transformation mechanisms of the [eta], [gamma] and [theta] transition aluminas, Acta Crystallographica, B47 (1991) 617-630.
[11] G. Paglia, C. Buckley, A. Rohl, B. Hunter, R. Hart, J. Hanna, L. Byrne, Tetragonal structure model for boehmite-derived γ-alumina, Phys. Rev. B, 68 (2003) 144110.
[12] V.P. Pakharukova, D.A. Yatsenko, E.Y. Gerasimov, A.S. Shalygin, O.N. Martyanov, S.V. Tsybulya, Coherent 3D nanostructure of γ-Al2O3: Simulation of whole X-ray powder diffraction pattern, Journal of Solid State Chemistry, 246 (2017) 284-292.
[13] E.J.W. Verwey, The Crystal Structure of γ-Fe2O3 and γ-Al2O3, Zeitschrift für Kristallographie - Crystalline Materials, 91 (1935) 65-69.
[14] I. Levin, D. Brandon, Metastable alumina polymorphs: crystal structures and transition sequences, J American Ceramic Society, 81 (1998) 1995-2012.
[15] B. Ealet, M.H. Elyakhloufi, E. Gillet, M. Ricci, Electronic and Crystallographic Structure of Gamma-Alumina Thin-Films, Thin Solid Films, 250 (1994) 92-100.
[16] B.C. Lippens, J.H. de Boer, Study of phase transformations during calcination of aluminum hydroxides by selected area electron diffraction, Acta Crystallographica, 17 (1964) 1312-1321.
[17] J.A. Wang, X. Bokhimi, A. Morales, O. Novaro, T. Lopez, R. Gomez, Aluminum local environment and defects in the crystalline structure of Sol− Gel alumina catalyst, J. Phys. Chem. B, 103 299-303.
[18] M.H. Lee, C.F. Cheng, V. Heine, J. Klinowski, Distribution of tetrahedral and octahedral Al sites in gamma alumina, Chemical Physics Letters, 265 (1997) 673-676.
[19] C. Wolverton, K. Hass, Phase stability and structure of spinel-based transition aluminas, Physical Review B, 63 (2000).

[20] G. Gutiérrez, A. Taga, B. Johansson, Theoretical structure determination of γ−Al2O3, Physical Review B, 65 (2001) 1995-1994.
[21] H.P. Pinto, R.M. Nieminen, S.D. Elliott, Ab initio study of gamma-Al2O3 surfaces, Physical Review B, 70 (2004).
[22] E. Menéndez-Proupin, G. Gutiérrez, Electronic properties of bulk γ−Al2O3, Physical Review B, 72 (2005) 65-69.
[23] D.Y. Li, B.H. O'Conner, G.I.D. Roach, J.B. Cornell, XVth Congress of the International Union of Crystallography in, 1990.
[24] L. Smrcok, V. Langer, J. Krestan, γ-Alumina: a single-crystal X-ray diffraction study, Acta Cryst, 62 (2006) i83-i84.
[25] M. Digne, P. Sautet, P. Raybaud, P. Euzen, H. Toulhoat, Use of DFT to achieve a rational understanding of acid–basic properties of γ-alumina surfaces, Journal of Catalysis, 226 (2004) 54-68.
[26] R. Prins, Location of the Spinel Vacancies in γ-Al2O3, Angew. Chem. Int. Ed., 91 (2019) 65-66.
[27] A. Dauger, D. Fargeot, TEM. study of Al2O3 metastable phases, Radiation effects, 74 (1983) 279-289.
[28] W.F. Li, X.L. Ma, Y. Li, W.S. Zhang, W. Zhang, Z.D. Zhang, Stacking faults and polymorphs in alumina nanorods, Philosophical Magazine, 85 (2005) 3809-3821.
[29] S.V. Tsybulya, G.N. Kryukova, Nanocrystalline transition aluminas: Nanostructure and features of x-ray powder diffraction patterns of low-temperature Al2O3 polymorphs, Physical Review B, 77 (2008) 024112.
[30] L. Samain, A. Jaworski, M. Edén, D.M. Ladd, D.-K. Seo, F.J. Garcia-Garcia, U. Häussermann, Structural analysis of highly porous γ-Al2O3, Journal of Solid State Chemistry, 217 (2014) 1-8.
[31] G. Paglia, E.S. Božin, S.J.L. Billinge, Fine-Scale Nanostructure in γ-Al2O3, Chemistry of Materials, 18 (2006) 3242-3248.
[32] L. Kovarik, A. Genc, C. Wang, A. Qiu, C.H.F. Peden, J. Szanyi, J.H. Kwak, Tomography and High-Resolution Electron Microscopy Study of Surfaces and Porosity in a Plate-like γ-Al2O3, The Journal of Physical Chemistry C, 117 (2013) 179-186.
[33] E.J. Kirkland, Advanced Computing in Electron Microscopy, Springer, 2010.
[34] G. Kresse, J. Furthmüller, Efficiency of ab-initio total energy calculations for metals and semiconductors using a plane-wave basis set, Computational Materials Science, 6 (1996) 15-50.
[35] G. Kresse, D. Joubert, From ultrasoft pseudopotentials to the projector augmented-wave method, Physical Review B, 59 (1999) 1758.
[36] K. Khivantsev, N.R. Jaegers, J.H. Kwak, J. Szanyi, L. Kovarik, Precise Identification and Characterization of Catalytically Active Sites on the Surface of γ-Alumina**, Angewandte Chemie, 133 (2021) 17663-17671.
[37] L. Kovarik, M. Bowden, A. Andersen, N.R. Jaegers, N. Washton, J. Szanyi, Quantification of High‐Temperature Transition Al2O3 and Their Phase Transformations**, Angew. Chem. Int. Ed., 59 (2020) 21719-21727.
[38] L. Kovarik, M. Bowden, D. Shi, J. Szanyi, C.H.F. Peden, Structural Intergrowth in δ-Al2O3, The Journal of Physical Chemistry C, 123 (2019) 9454-9460.

[39] J.M. Howe, 14 - Structure, Composition and Energy of Solid–Solid Interfaces, in: D.E. Laughlin, K. Hono (Eds.) Physical Metallurgy (Fifth Edition), Elsevier, Oxford, 2014, pp. 1317-1451.
[40] L. Kovarik, M. Bowden, A. Genc, J. Szanyi, C.H.F. Peden, J.H. Kwak, Structure of δ-Alumina: Toward the Atomic Level Understanding of Transition Alumina Phases, The Journal of Physical Chemistry C, 118 (2014) 18051-18058.
[41] A.N. Shmakov, G.N. Kryukova, S.V. Tsybulya, A.L. Chuvilin, L.P. Solovyeva, Vacancy Ordering in [gamma]-Fe2O3: Synchrotron X-ray Powder Diffraction and High-Resolution Electron Microscopy Studies, J. Appl. Cryst., 28 (1995) 141-145.
[42] H.L. Andersen, B.A. Frandsen, H.P. Gunnlaugsson, M.R.V. Jorgensen, S.J.L. Billinge, K.M.O. Jensen, M. Christensen, Local and long-range atomic/magnetic structure of non-stoichiometric spinel iron oxide nanocrystallites, IUCrJ, 8 (2021) 33-45.
[43] C. Greaves, A powder neutron diffraction investigation of vacancy ordering and covalence in γ-Fe2O3, Journal of Solid State Chemistry, (1983).
[44] L. Kovarik, M. Bowden, D. Shi, N.M. Washton, A. Andersen, J.Z. Hu, J. Lee, J. Szanyi, J.H. Kwak, C.H.F. Peden, Unraveling the Origin of Structural Disorder in High Temperature Transition Al2O3: Structure of θ-Al2O3, Chemistry of Materials, 27 (2015) 7042-7049.
[45] S.J. Wilson, The dehydration of boehmite, γ-AlOOH, to γ-Al2O3, Journal of Solid State Chemistry, 30 (1979) 247-255.
[46] C. Pecharromán, I. Sobrados, J.E. Iglesias, T. González-Carreño, J. Sanz, Thermal evolution of transitional aluminas followed by NMR and IR spectroscopies, J. Phys. Chem. B, 103 (1999) 6160-6170.
[47] M. Schöneborn, J. Werner, T. Harmening, T.E. Weirich, Advances in the understanding of mesoporous transition aluminas: Unveiling the correlation between morphology and thermostability, Journal of Solid State Chemistry, 308 (2022) 122906.
[48] S. Xu, N.R. Jaegers, W. Hu, J.H. Kwak, X. Bao, J.S. Acs, High-Field One-Dimensional and Two-Dimensional 27Al Magic-Angle Spinning Nuclear Magnetic Resonance Study of θ-, δ-, and γ-Al2O3 Dominated Aluminum Oxides: Toward Understanding the Al Sites in γ-Al2O3, ACS Omega, 6 (2021) 4090-4099.
[49] H. Kraus, M. Müller, R. Prins, A.P.M. Kentgens, Comments on the 27Al NMR Visibility of Aluminas, J. Phys. Chem. B, 102 (1998) 3862-3865.
[50] C.S. John, N.C.M. Alma, G.R. Hays, Characterization of transitional alumina by solid-state magic angle spinning aluminium NMR, Appl Catal, 6 (1983) 341-346.
[51] J.Z. Hu, S. Xu, J.H. Kwak, M.Y. Hu, C. Wan, Z. Zhao, J. Szanyi, X. Bao, X. Han, Y. Wang, C.H.F. Peden, High field 27Al MAS NMR and TPD studies of active sites in ethanol dehydration using thermally treated transitional aluminas as catalysts, Journal of Catalysis, 336 (2016) 85-93.
[52] R. Wischert, P. Florian, C. Copéret, D. Massiot, P. Sautet, Visibility of Al surface sites of γ-alumina: A combined computational and experimental point of view, Journal of Physical Chemistry C, 118 (2014) 15292-15299.
[53] D. Fargeot, D. Mercurio, A. Dauger, Structural characterization of alumina metastable phases in plasma sprayed deposits, Chemical Physics Letters, 24 (1990) 299-314.
[54] K.J. Morrissey, K.K. Czanderna, R.P. Merrill, C.B. Carter, Transition Alumina Structures Studied Using HREM, Ultramicroscopy, 18 (1985) 379-385.

[55] T.J. Bastow, A. Trinchi, M.R. Hill, R. Harris, T.H. Muster, Vacancy ordering in γ-Fe2O3 nanocrystals observed by 57Fe NMR, Journal of Magnetism and Magnetic Materials, 321 (2009) 2677-2681.
[56] J.-E. Jørgensen, L. Mosegaard, L.E. Thomsen, T.R. Jensen, J.C. Hanson, Formation of γ-Fe2O3 nanoparticles and vacancy ordering: An in situ X-ray powder diffraction study, Journal of Solid State Chemistry, 180 (2007) 180-185.
[57] L. Kovarik, K. Khivantsev, M. Bowden, J. Szanyi, In-situ Observation of Ordering Transformations in θ-Al2O3, MAM, 27 (2021) 1956-1957.